High-Order Photon Rings around Kerr Naked Singularities

Hina Suzuki $^{\bullet}$, 1,2 Yosuke Mizuno $^{\bullet}$, 3,4,5 Akhil Uniyal $^{\bullet}$, 3 Indu Kalpa Dihingia $^{\bullet}$, 3 Tintin Nguyen $^{\bullet}$, and Chi-kwan Chan $^{\bullet}$, 1,7,8

¹Steward Observatory and Department of Astronomy, University of Arizona, 933 N. Cherry Ave., Tucson, AZ 85721, USA
 ²Department of Electrical and Computer Engineering, University of Arizona, 1230 E. Speedway Blvd., Tucson, AZ 85721, USA
 ³Tsung-Dao Lee Institute, Shanghai Jiao-Tong University, Shanghai, 1 Lisuo Road, 201210, People's Republic of China
 ⁴School of Physics & Astronomy, Shanghai Jiao-Tong University, Shanghai, 800 Dongchuan Road, 200240, People's Republic of China
 ⁵Key Laboratory for Particle Physics, Astrophysics and Cosmology (MOE), Shanghai Key Laboratory for Particle Physics and Cosmology, Shanghai Jiao-Tong University, 800 Dongchuan Road, Shanghai, 200240, China
 ⁶Center for Astrophysics | Harvard & Smithsonian, 60 Garden Street, Cambridge, MA 02138, USA
 ⁷Data Science Institute, University of Arizona, 1230 N. Cherry Ave., Tucson, AZ 85721, USA
 ⁸Program in Applied Mathematics, University of Arizona, 617 N. Santa Rita, Tucson, AZ 85721, USA

ABSTRACT

We present a detailed study of higher-order photon rings of an accreting Kerr naked singularity (KNS) with dimensionless spin parameter a=1.01; i.e., a horizonless, overly spinning compact object. Motivated by horizon-scale very-long-baseline interferometry (VLBI) including Event Horizon Telescope (EHT) and future missions such as the Black Hole Explorer (BHEX), we analyze image morphology and interferometric visibilities to identify observational signatures that differentiate KNS from Kerr black holes. We find that higher-order photon rings are tightly concentrated within the nominal "shadow" region and that the shadow develops a pronounced gap at sufficiently large observer inclination. These morphological differences produce measurable deviations in the complex visibilities relative to Kerr black hole predictions. Our results indicate that photon-ring structure and visibility-domain diagnostics at horizon-resolving baselines can provide a direct observational test of the presence (or absence) of an event horizon and thus offer a concrete avenue to test general relativity with future horizon-scale observations.

Keywords: Black Hole physics; Naked Singularities; Photon Rings; Radiative Transfer

1. INTRODUCTION

The Event Horizon Telescope (EHT) has opened a new era in experimental gravity, delivering the first horizon-scale images of supermassive black holes—M87* and Sagittarius A* (Sgr A*) (Event Horizon Telescope Collaboration et al. 2019a, 2022). These observations offer an unprecedented opportunity to test the prediction of general relativity (GR) in the strong field regime, particularly through the morphology of black hole shadows and associated photon rings (Johannsen & Psaltis 2010; Mizuno et al. 2018; Psaltis et al. 2020; Vagnozzi et al. 2023; Uniyal et al. 2025b).

Mainstream researches interpret these images by assuming that M87* and Sgr A* are Kerr black holes (KBH) with event horizons Event Horizon Telescope Collaboration et al. (2019b); The Event Horizon Telescope Collaboration (2023). However, these interpretations are not unique. Other compact objects, such

as Kerr naked singularities (KNSs) can produce similar shadow images, raising the question of whether horizonless spacetime should also be consistent with exciting observations (e.g., Collaboration 2019; Psaltis et al. 2020; Kocherlakota et al. 2021). Recently, Olivares et al. (2020) showed that a boson star can be distinguished from a black hole by comparing the image of a non-rotating boson star with Schwarzschild and rapidly spinning Kerr black hole. Therefore, it is important to study other compact objects, such as KNS, to understand how their images differ from those of black holes.

Naked singularities arise when the Kerr spin parameter exceeds the Kerr bound ($|a| \le 1.0$), where $a = J/M^2$ is the spin parameter of a compact object with mass M and its angular momentum J. Although traditionally, naked singularities were considered to be nonphysical objects due to the violation of the cosmic censorship conjecture, they have been studied as a candidate ob-

ject for testing the limits of classical GR and exploring the phenomenology of extreme gravity.

The weak cosmic censorship conjecture proposes that spacetime singularities resulting from gravitational collapse must be hidden from an observer at infinity by event horizons (Penrose 1969). If this is true, this would ensure that classical GR remains predictive in physically relevant spacetime. Violation of this principle would imply a fundamental breakdown of predictability in GR. However, multiple naked singularities can solve Einstein's field equations (Janis et al. 1968; Mizuno et al. 2016; Shapiro & Teukolsky 1991; Joshi et al. 2011; Crisford & Santos 2017). Theoretical studies have demonstrated that naked singularities can also arise in dynamical collapse, alternative gravity models, or semiclassical contexts. Their observational signatures—including altered shadow geometry, bright central regions, and enhanced photon ring structure—may offer a route to test this foundational principle empirically.

Prior works have investigated the shadow geometry and lensing signatures of naked singularities, using analytical or idealized ray-tracing models (e.g., Bambi & Freese 2009; Nguyen et al. 2023; Tavlayan & Tekin 2024; Kumar & Ghosh 2021; Hioki & Maeda 2009a). These studies have shown that the spins and observational inclination angles impact observable quantities of naked singularities, such as the arc length, angle, curvature radius, and distortion parameter of the shadow. These studies have established that KNSs can produce image structures similar to black holes, but with subtle differences in the morphology, brightness of photon rings, and brightness depression of the inner region. Recently, some general relativistic magnetohydrodynamic (GRMHD) simulations were performed to distinguish the KNS from the KBH (Dihingia et al. 2025), which further also investigated, along with other naked singularity solutions to know the strong outflow mechanism responsible around such compact objects (Unival et al. 2025a). An extensive study has been done to distinguish Reissner-Nordström (RN) naked singularities from their black hole counterparts (Mishra et al. 2024; Kluźniak & Krajewski 2024; Čemeljić et al. 2025). The intensity of the central brightness depressions in EHT images provides another way to distinguish black holes from other types of naked singularities, such as the Janis-Newman-Winicour and Gauss-Bonnet naked singularities (Deliyski et al. 2025).

High-order photon rings, formed by photons that orbit around the compact objects multiple times, carry detailed information about the spacetime geometry near the photon sphere (Gralla et al. 2020). These rings also provide a more sensitive test of spacetime structure than

the shadow boundary alone, which can be highly sensitive to the accretion physics (Johnson et al. 2020). A major opportunity to probe the feature lies with the Black Hole Explorer (BHEX) mission, a space-VLBI designed to resolve high-order photon rings (Johnson et al. 2024). At a longer baseline length of $\sim 27G\lambda$ (~ 3 times higher angular resolution than the EHT), BHEX probes the interferometric regime where the first-order sub-ring becomes dominant for a KBH (Johnson et al. 2020).

To prepare for such high-precision tests of gravity, it is essential to understand the higher-order photon ring structure in both black holes and naked singularities' spacetime. In particular, the interpretation of BHEX observation will require robust forward modeling of horizonless geometries, including realistic emission and plasma dynamics. So far, this regime has remained largely unexplored, especially in the absence of realistic emission models.

In this paper, we present the first detailed study of higher-order photon rings around a KNS with general relativistic radiative transfer (GRRT) using GRMHD simulated data of KNSs. Building on recent progress in modeling accretion flow onto KNSs (Dihingia et al. 2025), we perform ray tracing through a 3D turbulent plasma to construct a synthetic image and isolate the cascaded photon rings. We shall calculate image of a high-order photon ring at various inclination angles. In order to provide observables with VLBI instruments, we plot visibility amplitude against u-v baseline distance. Our results provide predictive templates of high-resolution imaging and contribute to the development of strong-field tests of general relativity using future VLBI instruments.

The outline of the paper is as follows. In Sec. 2 we introduce the theoretical expectations for photon rings around KNS. In Sec. 3 we describe the GRRT simulation setup and the initial conditions used for the GRMHD models. In Sec. 4 we present the higher-order photon rings of KNS and their dependence on observer inclination. In Sec. 5 we compute and analyze the visibility amplitudes corresponding to these high-order rings. Finally, in Sec. 6 we summarize our findings and discuss implications for observational tests of horizonless spacetimes.

2. THEORETICAL EXPECTATION FOR PHOTON "RINGS" AROUND KNS

2.1. Critical Curve and Photon Ring

Below, we review some technical details regarding photon rings to clarify key terminologies and subsequent calculations. The interested readers could refer to the review by Lupsasca et al. 2024 for derivations and further

details. Kerr spacetime admits several conserved quantities along null geodesics: energy E, azimuthal angular momentum L, and Carter's constant C (Carter 1968). Spherical photon orbits (at constant radius $r=\tilde{r}$) are characterized by conserved quantities $\Phi \equiv L_z/E$ and $Q \equiv C/E^2$ in the following set of equations (Teo 2003):

$$\Phi = -\frac{\tilde{r}^3 - 3\tilde{r}^2 + a^2\tilde{r} + a^2}{a(\tilde{r} - 1)}$$
 (1)

$$Q = \frac{\tilde{r}^3(\tilde{r}^3 - 6\tilde{r}^2 + 9\tilde{r} - 4a^2)}{a^2(\tilde{r} - 1)^2}$$
 (2)

A photon with conserved quantities Φ and Q can be projected to an image plane at infinity at an inclination angle i from the spin axis with Cartesian coordinates (x, y) (or equivalently α, β in Bardeen 1973):

$$x = -\Phi \csc i \tag{3}$$

$$y = \pm \sqrt{Q + a^2 \cos^2 i} - \Phi^2 \cot^2 i \tag{4}$$

Unstable spherical photon orbits around KNSs exist in the range $r_{\rm ms} < r < r_{\rm ph}$, where $r_{\rm ms}$ and $r_{\rm ph}$ are the marginally stable orbital radius and the equatorial retrograde circular orbital radius, respectively (Charbulák & Stuchlík 2018):

$$r_{\rm ms} = 1 + (a^2 - 1)^{1/3}$$
 (5)

$$r_{\rm ph} = 2 + 2 \cosh \left[\frac{1}{3} \cosh^{-1} (2a^2 - 1) \right]$$
 (6)

The projection of unstable spherical photon orbits to an observer at infinity through Equations 1-6 trace out the critical curve on the image plane. For KBH, the critical curve is a closed boundary separating the interior region of photon capture (the black hole shadow) and the exterior region of photon escape. For KNS, the critical curve may develop a gap or not exist for higher viewing inclination and spin (Nguyen et al. 2023). By definition, the critical curve is an infinitely thin region of bound orbits that cannot be detected by our telescope. Equating the critical curve and the black hole shadow to the central brightness depressions in EHT images requires strong astrophysical assumptions on the accretion physics, thus posing limitations in probing spacetime properties and strong-field tests of gravity.

In practice, the observable photon ring is an infinite series of self-similar sub-rings formed by nearly bound orbits, where each sub-ring is indexed by its image order n, denoting the number of half orbits the photon make around the KBH or KNS (Gralla et al. 2019a). Each successive sub-ring (increasing image order in n) converges exponentially towards the critical curve at the limit of $n \to \infty$ and becomes exponentially thinner in

width (Johnson et al. 2020), making them prime targets of space-based VLBI. For example, BHEX aims to resolve the first-order (n=1) photon rings of M87* and Sgr A* (Johnson et al. 2024).

2.2. Comparison Between KNS and KBH Photon Rings

It is expected that the photon rings around KNS would show significant differences from their black hole counterparts because of the non-existence of the event horizon and the reflective nature of the KNS. For KBHs, the observed photon ring remains essentially circular for any spin parameter and observer inclination (Psaltis 2019). The spacetime admits both prograde and retrograde unstable photon trajectories, and their projection on the image plane produces a continuous, closed shadow silhouette. Therefore, in the case of black holes, with an event horizon, cascaded photon rings converge into a critical curve, the projection of the unstable photon orbit onto the image plane of the distant stationary observer (Gralla et al. 2019b).

In contrast, for the case of the KNS, a subset of prograde photon paths confined to the equatorial plane (and nearby spherical orbits) do not continue to form bound, scattering trajectories but instead spiral into the central singularity or escape to infinity by passing through the inside of a singular ring, leaving behind a dark spot or line depending on the inclination angle. On the other hand, the retrograde unstable photon trajectories produce an arc-like image since they can come back to the observer (Hioki & Maeda 2009b; Patel et al. 2022). Now, in the realistic case, because KNS lack an event horizon, the region that would correspond to the black-hole "shadow" is expected to be filled by a highly lensed image of the accretion flow rather than remaining dark. Hence, photon rings exterior to the critical curve are expected to resemble those of black holes, but the nominal shadow interior will generally contain lensed emission. Nguyen et al. (2023); Dihingia et al. (2025) have shown that, for sufficiently high spin and near edgeon inclinations, the photon rings can develop an earlier discussed gap, and for larger spin or inclination, the rings may disappear entirely. How emission is lensed through or across this gap remains an open theoretical problem. However, higher-order photon images should behave qualitatively differently because there is no horizon to absorb light; hence, whenever an n-order image appears outside the critical curve, a corresponding counterpart is expected to appear inside the curve. We have discussed this in detail in the following sections.

3. NUMERICAL SETUP

This study analyzes the geometry of high-order photon rings using a dataset from 3D GRMHD simulations performed with the BHAC code (Porth et al. 2017; Olivares et al. 2019) in modified Kerr–Schild coordinates (Details of GRMHD simulation can be found at: Dihingia et al. 2025). For the GRMHD simulation, an "inflow" boundary condition has been adopted at the inner boundary of the simulation outside the naked singularity at $r = 0.3680 r_q$. Note that the results from the GRMHD simulations become independent of whether the inner boundary is "inflow" or "reflective" if the boundary is close enough to the singularity (see Appendix B of Dihingia et al. (2025)). We extract 400 snapshots over the simulation ranging from t = $1000\,t_q - 5000\,t_q$ and compute ray-traced images using a relativistic radiative transfer code, RAPTOR (Bronzwaer et al. 2018, 2020). The source is considered Sgr A*, having mass $M = 4.14 \times 10^6 M_{\odot}$ at distance 8.127 kpc. By choosing $R_{high} = R_{low} = 1$ for simplicity, we assume a single-temperature plasma emission exclusively from thermal synchrotron radiation. We also rescale the mass accretion rate to produce an optically thin image, ensuring that the emission becomes transparent at 230 GHz so that the underlying photon-ring structure can be robustly identified and analyzed in image domain. We calculated images with the grid resolution in the image plane being 1000×1000 pixels, and the field of view 40 r_g^2 (0.25 mas²). Figures 1 and 2 show time averaged images in $8 r_a^2 (0.05 \text{ mas}^2)$ for visualization.

For a better comparison, we considered a range of inclination angles of observers placed at i = $[15^{\circ}, 30^{\circ}, 45^{\circ}, 60^{\circ}, 75^{\circ}].$ The images are calculated at 230 GHz to match the EHT observing frequency. Each image is normalized and visualized in a quadratic scale for better compari-Furthermore, we used the publicly available eventhorizontelescope/2017-sgra-paper5 pipeline to compute visibility amplitude curves consistent with EHT data products. Sub-ring decomposition is performed by isolating photon trajectories based on their half-winding number around the KNS. We analyze the contribution of each sub-ring to the total image and study its visibility signatures in the uv domain.

4. HIGH-ORDER PHOTON RING AROUND KNS

In this section, we computed images of KNS at different observer inclinations and examine how the higher-order photon rings change with inclination. Figure 1 shows the higher-order photon rings for KNS at inclination angle $i=60^{\circ}$. The blue curve denotes the critical curve, analytically computed with Equations 1-

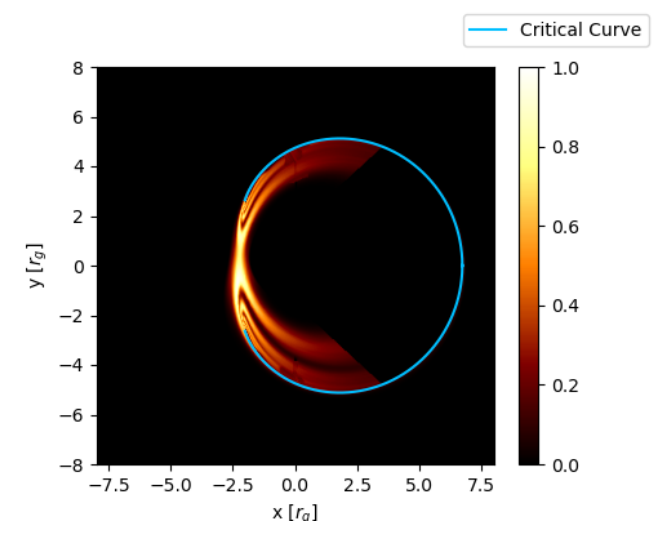


Figure 1. High-Order Photon ring structure around a KNS with spin a=1.01 and a polar inclination angle $i=60^{\circ}$, ray-traced from 3D GRMHD simulation data from (Dihingia et al. 2025). The critical curve is calculated with the analytical calculations (Equations 1-6). Multiple cascaded photon rings appear on both sides of the critical curve (blue) due to the absence of an event horizon. Inner rings are thicker and more sparse, connected with outer rings around the equatorial plane. Intensity is normalized and visualized on a quadratic scale to enhance the visibility of the sub-ring. Dark regions on the right side are likely artifacts from the numerical boundary in the simulation and do not affect the analysis of the VLBI observational signature.

6. Unlike the nearly circular photon rings seen around KBH, the KNS produces a pronounced, multilayered thick—ring structure. Because there is no event horizon, rings appear both inside and outside the critical curve and connect across the equatorial plane, with the inner cascades appearing broader and more sparsely spaced. For clarity, all intensities are normalized and displayed using a quadratic intensity scaling to enhance the faint, high-order features. To compensate for the numerical limitation along the polar axis in GRRT calculations, we interpolate along a distorted radial coordinate defined with respect to the critical curve. ¹

The dark regions visible on the right of the figure are most likely artifacts caused by the finite inner boundary of the GRMHD simulation, which was imposed for com-

¹ Interpolation was performed along the azimuthal direction ϕ on a coordinate system defined by the critical curve. The distorted coordinate were constructed from cartesian (x,y) to distorted polar coordinate (r,ϕ) as $r=\sqrt{x^2+y^2}/r_{\rm crit}(\phi)$ and $\phi=\tan^{-1}(y/x)$, where $r_{\rm crit}$ is the radius of critical curve as a function of ϕ . The values were interpolated using the scipy.interpolate.griddata function with the linear method, which performs piecewise linear interpolation between neighboring data points.

putational reasons. Although the inner boundary can in principle be moved closer to the singularity (r=0), the overall dynamics is insensitive to this choice for our case because the KNS is modeled with a reflective inner boundary (Dihingia et al. 2025; Uniyal et al. 2025a), therefore, does not impact our VLBI observational signature of the KNS.

Figure 2 shows the decomposition of sub-rings and their contribution to the total image at different inclinations. The right-most panels represent the clear structure of the higher-order rings for each inclination angle. For all inclination angles, we observe two rings on both inside and outside of the critical curve. We find that a gap in the left of a ring structure only appears for higherorder photon rings $(n \geq 2)$ and at sufficiently large inclinations $(i > 30^{\circ})$, where the gap begins to open up. KNSs are super-spinning (a > 1), so prograde photons that co-rotate with the spacetime can acquire sufficiently large effective angular momentum that the centrifugal barrier prevents them from maintaining bound (spherical) orbits (Charbulák & Stuchlík 2018). For a fixed spin, increasing the observer inclination from face-on toward edge-on increases the photon's motion in the ϕ direction and thus increases the magnitude of their effective angular momentum. This drives prograde trajectories to become progressively more prograde, and once those trajectories can no longer sustain spherical orbits, they produce a gap in the critical curve at sufficiently large inclinations. In particular, for a = 1.01 (Nguyen et al. 2023) indicates that the critical curve begins to open a gap at viewing angles roughly $i \gtrsim 31^{\circ}$.

The critical curve itself is an unobservable, infinitesimally thin locus, but photons emitted just outside it trace nearly bound trajectories that orbit arbitrarily close to the photon sphere. This behavior is evident in Figure 2, where the gap that first appears on the critical curve is already manifest in the n=2 images. By contrast, n=1 photons complete only roughly half an orbit around the KNS and therefore do not experience the same centrifugal barrier-driven removal. Consequently, the n=1 sub-ring does not develop a gap. Additionally, because the n=1 ring is slightly offset from the critical curve, we do not see a gap in the n=1 image for n=101 at n=102. In any case, whether a gap presents or not, the inner and outer ring components join smoothly at the edge of the critical curve.

5. VLBI SIGNATURE

In the previous section, we discussed how the higherorder rings show a gap with the different inclination angles, which is not present in the case of the BHs. We next examine the visibility-domain signatures of the higherorder rings to quantify their observational appearance. VLBI arrays detect a complex visibility $V(\mathbf{u})$, which is the Fourier transform of the corresponding the Sky image $I(\mathbf{x})$ (Thompson et al. 2017).

$$V(\mathbf{u}) = \int I(\mathbf{x})e^{-2\pi i\mathbf{u}\cdot\mathbf{x}}d\mathbf{x}$$
 (7)

, where **u** in (λ) is baseline vector projected orthogonal onto the line of sight, and **x** in (radians) is image coordinate. For the case of a thin, uniform, circular ring, image and visibility function on the observer plane, in polar coordinates (r, φ) , is

$$I(r,\varphi) = \frac{1}{\pi d}\delta(r - \frac{d}{2}) \tag{8}$$

$$V(u,\varphi_u) = J_0(\pi du) \tag{9}$$

Here, J_m are mth Bessel functions of first kind. Figure 3 shows the normalized visibility amplitude (Jy) as a function of baseline length $(G\lambda)$ for the decomposed sub-rings and for the full image at different inclinations.

Visibilities are computed from 0 to 200 $G\lambda$. The visibility oscillation frequency reflects the characteristic ring diameter, while the oscillation envelope exhibits only weak decay across photon-ring orders. This slow fall-off arises because the emission in the KNS images is extended rather than concentrated in an infinitely thin ring. Thus, significant power remains at high spatial frequencies even for higher-order sub-rings compared to the BHs (Wong et al. 2024; Capistrano et al. 2025).

6. DISCUSSION

In this work, we have carried out a systematic study of simulated images of accreting KNSs and contrasted their appearance with that of KBHs. Our analysis identifies several distinct morphological and radiative signatures that arise from the absence of an event horizon, providing potential observational diagnostics that can distinguish horizonless spacetimes.

We identified a cascaded photon-ring structure in which successive photon-ring orders form distinct, layered features. As the inclination angle increases, these rings develop a gap consistent with earlier theoretical predictions; however, the gap emerges only in the higher-order components of the image. This is highly relevant to future space-based VLBI mission such as BHEX, which can only probe the n=1 photon ring of M87* and Sgr A*. Even for KNS models where the critical curve (or higher-order sub-rings at $n \geq 2$) opens a gap (e.g, $a=1.01, i \gtrsim 30^\circ$ models), they cannot be ruled out by EHT and BHEX observations of a closed photon ring image dominated by lower-order (n=0 and n=1)

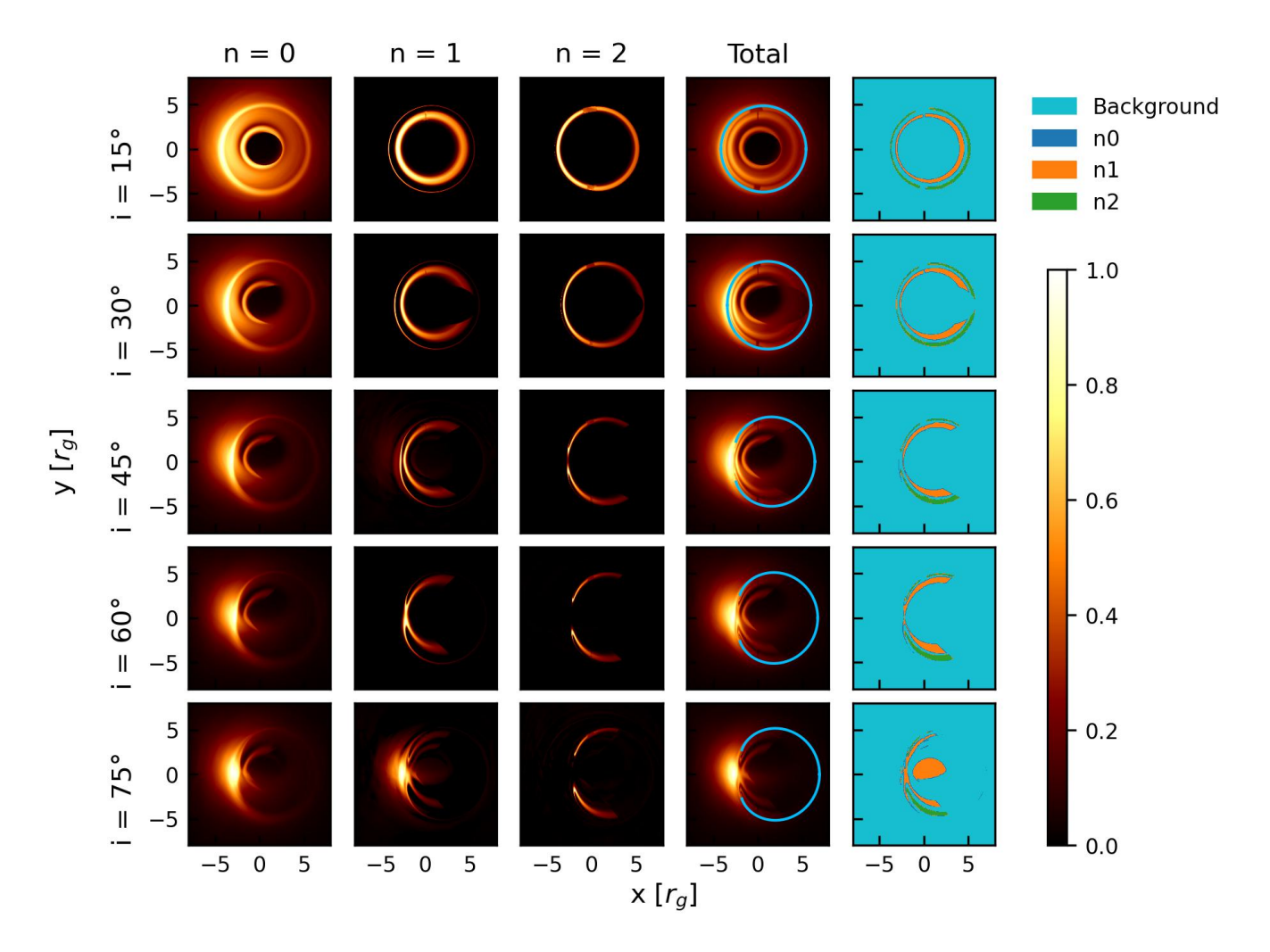


Figure 2. Decomposition of the sub-rings at different inclinations. Two cascaded rings per order of photon ring appear on both sides of the critical curve. For all inclination angles, rings inside the critical curve have a thicker profile than those outside. At the higher inclination angles, high-order photon rings begin to open a gap. The right panels display the spatial contribution of each sub-ring to the total image. Similar to KBH, the intensity decreases as the order of the photon ring increases, but the presence of inner rings introduces additional structure within the shadow region.

components. Conclusively ruling out KNS models such as $a=1.01,\ i\gtrsim 30^\circ$ based on whether an observed photon ring image develops a gap or not requires much longer baseline at $\gtrsim 200\ {\rm G}\lambda$ (e.g. on the Moon) to probe n=2 photon rings.

These morphological differences produce distinctive visibility-domain signatures, suggesting that interferometric observations at horizon-scale resolution could potentially distinguish KNS from KBH images. In particular, the cascaded photon-ring structure and the inclination-dependent gap are likely to induce measurable modulations in the visibility amplitude accessible to next-generation VLBI facilities (e.g., BHEX). The absence of the event horizon produces a thicker emission structure due to the inner ring features. The width of each KNS sub-ring becomes thinner for each succes-

sive order at a slower rate than KBH sub-rings, resulting in similar decay rates of the visibility amplitude across sub-rings, in contrast to the sharper fall-off observed in that of KBHs. As a consequence, whereas each progressively longer baseline regime is dominated by the emission of a single sub-ring at a particular image order for KBHs (Johnson et al. 2020), different KNSs sub-rings are not cleanly separated in the visibility response at longer baselines, as seen in Figure 3.

The extension of this work includes surveying a wider range of spin parameters, incorporating polarized radiative transfer to characterize polarization signatures near the gap and inside the critical curve, and studying time-dependent behavior and correlations. A complementary approach with isolating emission from the nominal shadow region and analyzing residual should

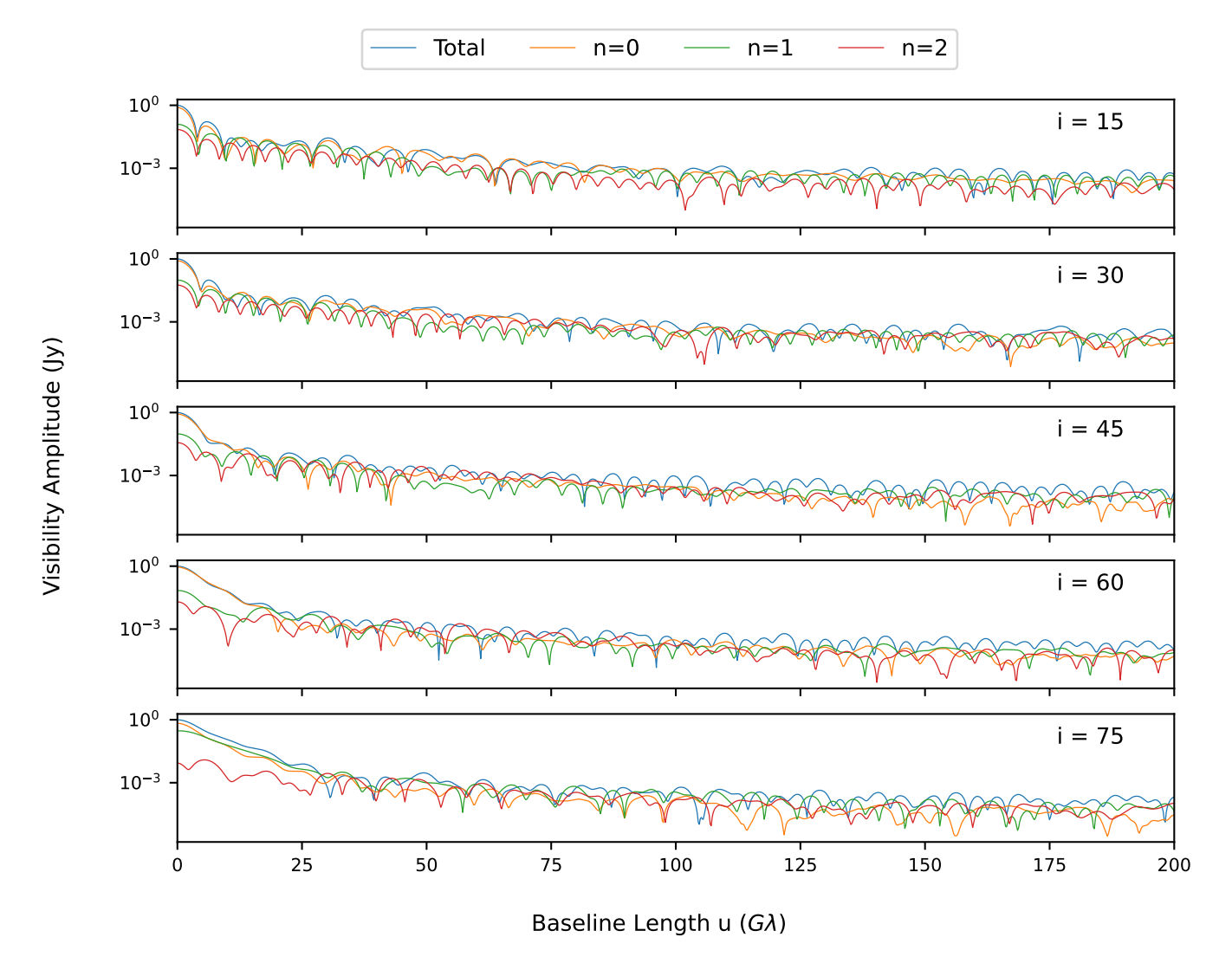


Figure 3. Normalized visibility amplitude of KNS (a = 1.01) as a function of (u, v)-distance for five inclination angles, shown from top to bottom. Each curve represents the amplitude from cascaded sub-rings. The absence of an event horizon produces a thicker emission structure, resulting in similar decay rates of the visibility amplitude across sub-rings compared to the sharper fall-off seen in that of black holes.

help quantify the fundamental morphological differences between KNS and KBH models. Finally, mapping the image morphologies across spin and inclination will allow a direct comparison between our GRMHD-based ray-tracing results and analytic predictions, providing a more comprehensive test of horizonless spacetime phenomenology. We planned to do it in the future.

Therefore, by linking GRMHD-based numerical simulations with analytic geodesic structures, this work provides a unified theoretical framework for distinguishing

black holes from naked singularities through their observable image features.

ACKNOWLEDGMENTS

Y.M., I.K.D., and A.U. are supported by the National Key R&D Program of China (Grant No. 2023YFE0101200), the National Natural Science Foundation of China (Grant No. 12273022), the Research Fund for Excellent International PhD Students (grant No. W2442004) and the Shanghai Municipality orientation program of Basic Research for International Scientists (Grant No. 22JC1410600). I.K.D. acknowledges the TDLI postdoctoral fellowship for financial support.

REFERENCES

- Bambi, C., & Freese, K. 2009, Phys. Rev. D, 79, 043002, doi: 10.1103/PhysRevD.79.043002
- Bardeen, J. M. 1973, in Black Holes (Les Astres Occlus), ed. C. Dewitt & B. S. Dewitt, 215–239
- Bronzwaer, T., Davelaar, J., Younsi, Z., et al. 2018, A&A, 613, A2, doi: 10.1051/0004-6361/201732149
- Bronzwaer, T., Younsi, Z., Davelaar, J., & Falcke, H. 2020, A&A, 641, A126, doi: 10.1051/0004-6361/202038573
- Capistrano, A. J. S., Gutierrez-Pineres, A. C., & Coimbra-Araujo, C. H. 2025. https://arxiv.org/abs/2510.07476
- Carter, B. 1968, Physical Review, 174, 1559, doi: 10.1103/PhysRev.174.1559
- Čemeljić, M., Kluźniak, W., Mishra, R., & Wielgus, M. 2025, ApJ, 981, 69, doi: 10.3847/1538-4357/adb421
- Charbulák, D., & Stuchlík, Z. 2018, Eur. Phys. J. C, 78, 879, doi: 10.1140/epjc/s10052-018-6336-5
- Collaboration, E. H. T. 2019, The Astrophysical Journal Letters, 875, L5, doi: 10.3847/2041-8213/ab0f43
- Crisford, T., & Santos, J. E. 2017, Phys. Rev. Lett., 118, 181101, doi: 10.1103/PhysRevLett.118.181101
- Deliyski, V., Gyulchev, G., Nedkova, P., & Yazadjiev, S. 2025, Phys. Rev. D, 111, 064068, doi: 10.1103/PhysRevD.111.064068
- Dihingia, I. K., Uniyal, A., & Mizuno, Y. 2025, ApJ, 978, 44, doi: 10.3847/1538-4357/ad9600
- Event Horizon Telescope Collaboration, Akiyama, K., Alberdi, A., et al. 2019a, ApJ, 875, L1, doi: 10.3847/2041-8213/ab0ec7
- —. 2019b, ApJ, 875, L6, doi: 10.3847/2041-8213/ab1141
- —. 2022, ApJ, 930, L12, doi: 10.3847/2041-8213/ac6674
- Gralla, S. E., Holz, D. E., & Wald, R. M. 2019a, Physical Review D, 100, 024018,
- doi: 10.1103/PhysRevD.100.024018
- —. 2019b, Phys. Rev. D, 100, 024018, doi: 10.1103/PhysRevD.100.024018
- Gralla, S. E., Lupsasca, A., & Marrone, D. P. 2020, Phys. Rev. D, 102, 124004, doi: 10.1103/PhysRevD.102.124004
- Hioki, K., & Maeda, K.-i. 2009a, Phys. Rev. D, 80, 024042, doi: 10.1103/PhysRevD.80.024042
- —. 2009b, Phys. Rev. D, 80, 024042, doi: 10.1103/PhysRevD.80.024042
- Janis, A. I., Newman, E. T., & Winicour, J. 1968, Phys. Rev. Lett., 20, 878,
 - doi: 10.1103/PhysRevLett.20.878
- Johannsen, T., & Psaltis, D. 2010, ApJ, 718, 446, doi: 10.1088/0004-637X/718/1/446
- Johnson, M. D., et al. 2020, Sci. Adv., 6, eaaz1310, doi: 10.1126/sciadv.aaz1310

- Johnson, M. D., Akiyama, K., Baturin, R., et al. 2024, in Society of Photo-Optical Instrumentation Engineers (SPIE) Conference Series, Vol. 13092, Space Telescopes and Instrumentation 2024: Optical, Infrared, and Millimeter Wave, ed. L. E. Coyle, S. Matsuura, & M. D. Perrin, 130922D, doi: 10.1117/12.3019835
- Joshi, P. S., Malafarina, D., & Narayan, R. 2011, Classical and Quantum Gravity, 28, 235018, doi: 10.1088/0264-9381/28/23/235018
- Kluźniak, W., & Krajewski, T. 2024, Phys. Rev. Lett., 133, 241401, doi: 10.1103/PhysRevLett.133.241401
- Kocherlakota, P., et al. 2021, Phys. Rev. D, 103, 104047, doi: 10.1103/PhysRevD.103.104047
- Kumar, R., & Ghosh, S. G. 2021, Classical and Quantum Gravity, 38, 085010, doi: 10.1088/1361-6382/abdd48
- Lupsasca, A., Mayerson, D. R., Ripperda, B., & Staelens,
 S. 2024, arXiv e-prints, arXiv:2402.01290,
 doi: 10.48550/arXiv.2402.01290
- Mishra, R., Krajewski, T., & Kluźniak, W. 2024, Phys. Rev. D, 110, 124030, doi: 10.1103/PhysRevD.110.124030
- Mizuno, R., Ohashi, S., & Shiromizu, T. 2016, Progress of Theoretical and Experimental Physics, 2016, 103E03, doi: 10.1093/ptep/ptw147
- Mizuno, Y., Younsi, Z., Fromm, C. M., et al. 2018, Nature Astron., 2, 585, doi: 10.1038/s41550-018-0449-5
- Nguyen, B., Christian, P., & Chan, C.-k. 2023, ApJ, 954, 78, doi: 10.3847/1538-4357/ace697
- Nguyen, B., Christian, P., & Chan, C.-k. 2023, The Astrophysical Journal, 954, 78, doi: 10.3847/1538-4357/ace697
- Olivares, H., Porth, O., Davelaar, J., et al. 2019, A&A, 629, A61, doi: 10.1051/0004-6361/201935559
- Olivares, H., Younsi, Z., Fromm, C. M., et al. 2020, Mon. Not. Roy. Astron. Soc., 497, 521, doi: 10.1093/mnras/staa1878
- Patel, V., Tahelyani, D., Joshi, A. B., Dey, D., & Joshi,
 P. S. 2022, Eur. Phys. J. C, 82, 798,
 doi: 10.1140/epjc/s10052-022-10638-w
- Penrose, R. 1969, Nuovo Cimento Rivista Serie, 1, 252
 Porth, O., Olivares, H., Mizuno, Y., et al. 2017,
 Computational Astrophysics and Cosmology, 4, 1,
 doi: 10.1186/s40668-017-0020-2
- Psaltis, D. 2019, Gen. Rel. Grav., 51, 137, doi: 10.1007/s10714-019-2611-5
- Psaltis, D., Medeiros, L., Christian, P., et al. 2020,Phys. Rev. Lett., 125, 141104,doi: 10.1103/PhysRevLett.125.141104
- Psaltis, D., et al. 2020, Physical Review Letters, 125, 141104, doi: 10.1103/PhysRevLett.125.141104

- Shapiro, S. L., & Teukolsky, S. A. 1991, Phys. Rev. Lett., 66, 994, doi: 10.1103/PhysRevLett.66.994
- Tavlayan, A., & Tekin, B. 2024, Classical and Quantum Gravity, 41, 065004, doi: 10.1088/1361-6382/ad2318
- Teo, E. 2003, General Relativity and Gravitation, 35, 1909, doi: 10.1023/A:1026286607562
- The Event Horizon Telescope Collaboration. 2023, arXiv e-prints, arXiv:2311.09484, doi: 10.48550/arXiv.2311.09484
- Thompson, A. R., Moran, J. M., & Swenson, Jr., G. W. 2017, Interferometry and Synthesis in Radio Astronomy, 3rd Edition, doi: 10.1007/978-3-319-44431-4

- Uniyal, A., Dihingia, I. K., Mizuno, Y., & Kluźniak, W. 2025a, Astrophys. J., 993, 97, doi: 10.3847/1538-4357/ae071a
- Uniyal, A., Dihingia, I. K., Mizuno, Y., & Rezzolla, L. 2025b, Nature Astronomy, 1, doi: 10.1038/s41550-025-02695-4
- Vagnozzi, S., Roy, R., Tsai, Y.-D., et al. 2023, Classical and Quantum Gravity, 40, 165007, doi: 10.1088/1361-6382/acd97b
- Wong, G. N., Medeiros, L., Cárdenas-Avendaño, A., & Stone, J. M. 2024, Astrophys. J. Lett., 975, L40, doi: 10.3847/2041-8213/ad8650